Applied Catalysis B: Environmental 164 (2015) 344–351

Contents lists available at ScienceDirect

Applied Catalysis B: Environmental

journal homepage: www.elsevier.com/locate/apcatb

Efficiently photocatalytic reduction of carcinogenic contaminant Cr (VI) upon robust AgCl:Ag hollow nanocrystals

Hongyan Li[a,c], Tongshun Wu[a], Bin Cai[a,c], Weiguang Ma[a,c], Yingjuan Sun[b,c], Shiyu Gan[a,c], Dongxue Han[a,*], Li Niu[a]

[a] State Key Laboratory of Electroanalytical Chemistry, c/o Engineering Laboratory for Modern Analytical Techniques, Changchun Institute of Applied Chemistry, Chinese Academy of Sciences, Changchun, 130022, Jilin, China
[b] State Key Laboratory of polymer physics and chemistry, Changchun Institute of Applied Chemistry, Chinese Academy of Sciences, Changchun, 130022, Jilin, China
[c] University of Chinese Academy of Sciences, Beijing, 100049, China

ARTICLE INFO

Article history:
Received 20 July 2014
Received in revised form
16 September 2014
Accepted 22 September 2014
Available online 28 September 2014

Keywords:
Photocatalysis
Plasma chemistry
Semiconductors
Hexavalent chromium (Cr (VI))
Schottky junction

ABSTRACT

Herein, we newly present a robust photocatalyst in terms of AgCl:Ag-Hollow nanocrystals (NCs) which exhibit fast photoreduction rate for representative carcinogenic contaminant (Cr (VI)) into the benign form(10 min). The provided hollow structure significantly enhanced light absorption and specific surface area (42 times than normal AgCl material), which are the two critical factors to improve the photoreduction activity. Further, the Schottky junction of the plasmonic system facilitates separation of photo-induced electrons and holes, which absolutely benefits the photocatalysis reactions. The photocurrent intensity, kinetic responses with apparent kinetic rate constant (k_{app}) and apparent quantum efficiency (AQE) (within 6 min) of AgCl:Ag-Hollow NCs were about 4–8, 5.3 and 2.7 times as that of normal AgCl material, respectively. Most strikingly, we anticipate such AgCl:Ag-Hollow NCs might become a promising candidate for practical application of water cleansing and environmental pollution purifying under visible light irradiation in the future.

1. Introduction

Over the past decades, semiconductor-based photocatalysis has been a hot research field due to its potential applications in coping with the energy crisis as well as environment pollution [1–6]. With unceasingly increasing industrial development after industrial revolution, carcinogenic hexavalent chromium (Cr (VI)) pollution incident continuously challenges our fragile living environment, especially the precious water resource that human beings live and depend on. It is well known that Cr (VI) is a frequent contaminant in wastewater arising from industrial processes such as leather tanning, paint making, electroplating and chromate production, etc. [7,8]. What troubled most is that the Cr (VI) ions can easily invade the human food chains and gradually accumulate to toxic levels, which becomes the main source of carcinogen and mutagenic primer [9]. Hence, multifarious conventional techniques for the removal of Cr (VI) have been reported, including biochemistry treatment, ion exchange, membrane separation, precipitation and adsorption, etc. [10]. Nevertheless, these approaches commonly subject to large requirement of chemicals, extra organic additives, high cost, and secondary pollution, all of which greatly hinder their practical applications. Consequently, pursuing environmental friendly and efficient technologies for cleaning Cr (VI)-containing wastewater has become an urgent task. Compared with those methods, photocatalysis has been proved to be a more attractive, efficient and clean strategy for reduction of toxic Cr (VI) species into the less harmful benign form, which is of paramount importance for human health [9,11].

Recently, there arose several research works concerning on photoreduction of Cr (VI) contaminants [12,13]. Unfortunately, those photocatalysts are far from commercial applications due to their long-term preparation process and low efficiency. To date, few works have been reported on plasmonic photocatalyst with well-defined morphology and excellent performance for photoreduction of Cr (VI) into the benign form. In this case, in the previous investigations, we have contributed a lot of theoretical and experimental efforts to study and improve the silver halide (AgX (X = Cl, Br, I)) based plasmonic photocatalysis, such as manipulation of the energy band structure and amelioration of the active crystal plane or hierarchical structure [11,14]. However, there still remains an immense

* Corresponding author. Tel.: +86 43185262425; fax: +86 43185262800.
E-mail addresses: dxhan@ciac.ac.cn, handongxue1206@gmail.com (D. Han).

http://dx.doi.org/10.1016/j.apcatb.2014.09.049
0926-3373/

space for further development of the AgX-based plasmonic photocatalysis [15,16]. To meet the high engineering requirements of the solar-powered sewage treatment, the catalytic efficiency and chemical durability of photocatalyst are the two key factors to be crucially solved [17,18]. Thanks to its facile plasmonic properties, superb photocatalysis properties and photo-stabilities, AgCl semiconductor material is considered to be one of the most promising candidates to break through this bottleneck [19,20].

Consequently, in the present work, we newly introduced a kind of AgCl:Ag-Hollow NCs which has been proved to be a robust plasmonic photocatalytic reduction agent to reduce the Cr (VI) into the Cr (III) via a facile and handy preparation approach. By means of the colorimetrical diphenylcarbazide (DPC) method [21], the photocatalytic activity for reduction of Cr (VI) contaminants has been investigated and showed that such NCs could facilely clean the Cr (VI)-containing waste water within 10 min. Furthermore, a novel and in-depth perspective of photocatalytic reduction mechanism for the reduction of Cr (VI) on the AgCl:Ag-Hollow NCs is proposed and discussed.

2. Experimental

2.1. Chemicals

Sodium chloride (NaCl) and Polyvinylpyrrolidone (PVP) were purchased from Sigma-Aldrich and used without further purification. Silver nitrate ($AgNO_3$) and Potassium bichromate ($K_2Cr_2O_7$) were obtained from Sinopharm Chemical Reagent (Shanghai, China) and used as received. All aqueous solutions were prepared with ultra-pure water (>18.2 MΩ cm) from a Milli-Q Plus system (Millipore). All glassware used in the following procedures were cleaned in a bath of freshly prepared HCl:HNO_3 (3:1, aqua regia) and rinsed thoroughly by water prior to use.

2.2. Preparation of AgCl:Ag-Hollow NCs

The AgCl:Ag-Hollow NCs were prepared through a water soluble salt dissolution method according to previous reports with some modifications [19,20]. Briefly, $AgNO_3$ (0.17 g) and PVP (1.5 g) were dissolved in 20 mL absolute ethanol at ambient temperature with ultrasonication (the solution became deep brown). Then, the as-prepared NaCl saturated aqueous solution was injected into 100 mL absolute ethanol under vigorously magnetic stirring. Immediately, the white suspension granules were observed formed in the ethanol solution (NaCl cubic crystal). Soon afterwards, the above $AgNO_3$/PVP ethanol solution was poured into the NaCl ethanol suspension, and then, the mixture was around-the-clock stirred for 24 h to form NaCl@AgCl core–shell structure. Subsequently the obtained yellow colored NaCl@AgCl emulsion was placed into a breaker and irradiated by Xenon arc lamp (CHF-XM35-500 W, Beijing Trusttech Co. Ltd, China) light for 30 min to form NaCl@AgCl:Ag core–shell structure (the solution became purple). Finally, the purple suspension was treated by centrifugation (8500 rpm, 5 min) and the collections were washed with ultra-pure water for several times to remove PVP and residual ions (Na^+, NO_3^- and Cl^-), and the AgCl:Ag-Hollow purple NCs were achieved. For comparison, normal Ag/AgCl materials were prepared by mixing $AgNO_3$ (0.01 mol L^{-1}) and NaCl (0.01 mol L^{-1}) aqueous solution under stirring in ambient temerature. Some Ag NPs generated on the surface of AgCl during aforementioned Xenon arc lamp light irradiation. And the obtained Ag/AgCl material was denoted as AgCl-Normal for further control experiments.

2.3. Photocatalytic reduction hexavalent chromium

The carcinogen of Cr (VI) was photoreduced with as-prepared AgCl:Ag-Hollow NCs. In the whole process, the optical system for photoreduction was followed with similar that aforementioned above and equipped with a UV cutoff filter ($\lambda \geq 420$ nm), and the irradiation height was 15 cm. In a typical procedure, the as-prepared AgCl:Ag-Hollow NCs (20 mg) were well dispersed into 20 mL of Cr (VI) solution under ultrasonication (10 mg L^{-1} based on Cr (VI) in a dilute $K_2Cr_2O_7$ solution as the source of Cr (VI)) in a home-made reactor equipped with a cooling water circulator assembled to keep the whole reaction system maintaining at a constant temperature condition. Then, ethylene diamine tetraacetic acid (EDTA, 0.01 M) was injected into the mixture, and the pH of the reaction suspension was adjusted to 2.0 with $HClO_4$. Soon afterwards, the 0.02 M of color developing reagent of diphenylcarbazide (DPC) in acetone was added into the mixture, and the color of the mixture would turn into violet. The suspension was stirred for 30 min in the dark to reach adsorption–desorption equilibrium and then exposed to visible-light irradiation to start the photocatalysis. After the photoreduction experiment was triggered by irradiation of visible light, the solution of aliquots volume were periodically withdrawn from the reaction vessel and centrifuged to remove the photocatalyst powders. And the Cr (VI) reduction was measured based on the spectrophotometric colorimetrical DPC method (at $\lambda = 540$ nm) by using a UV-Vis spectrophotometer (ultra-pure water as reference). Normally, C_t is the concentration of Cr (VI) solution at time t, C_0 is the initial concentration (10 mg L^{-1}). The photocatalytic measurement mentioned above was repeated twice to ensure the reliability of the results. The reproducibility of the AgCl:Ag-Hollow NCs was also tested with the following procedure: the photocatalyst was washed with ultra-pure water and ethanol for several times after photoreduction and then retested in the fresh mixture solution of Cr (VI) under the same experimental conditions as mentioned above.

3. Results and discussion

3.1. Electronic images, crystal structure and photophysical properties

Morphology and element distribution of the as-prepared AgCl:Ag-Hollow NCs were investigated by SEM, TEM, HAADF-STEM and elemental mapping (Fig. 1). The mappings of present AgCl:Ag-Hollow NCs are colored to distinctly mark parts of the element distribution in this structure. Compared with the solubility of NaCl in water (26.5 wt%, 20 °C), its solubility in absolute ethanol (0.065 wt%, 20 °C) is much lower. Base on the fact, when a small amount of saturated aqueous solution of NaCl was injected into the absolute ethanol with ration volume, the reaction system would quickly turn into white color originated from precipitate of NaCl crystal. Subsequently, the $AgNO_3$/PVP in absolute ethanol was poured into the above-mentioned dispersion under vigorously magnetic stirring. Herein, PVP served as the capping agent to stabilize the generated AgCl particles and prevent agglomeration of the resultant [22]. The Ag NPs were generated on the surface of AgCl under visible light irradiation (Fig. 1a). The SEM images of the AgCl:Ag-Hollow NCs with different resolutions are shown in Fig. 1b–d. It is observed that the AgCl:Ag-Hollow NCs depicted hollow cubic structure, which might be benefited from the crystal morphology of NaCl in the synthesis phase (Fig. S1 in Supporting information) [23]. Obviously, the AgCl:Ag-Hollow NCs displayed uniform morphology with some pores on the shells. The TEM images (Fig. 1e) and elemental mapping images (Fig. 1f–h) could clearly reveal that both the Cl and Ag elements distributed on the cubic shell instead of center, which further proved the hollow structure obtained in such a AgCl:Ag material. In addition, the SEM and TEM images of the as-prepared AgCl:Ag-Hollow NCs with high resolution were corresponding performed. The pore and Ag^0

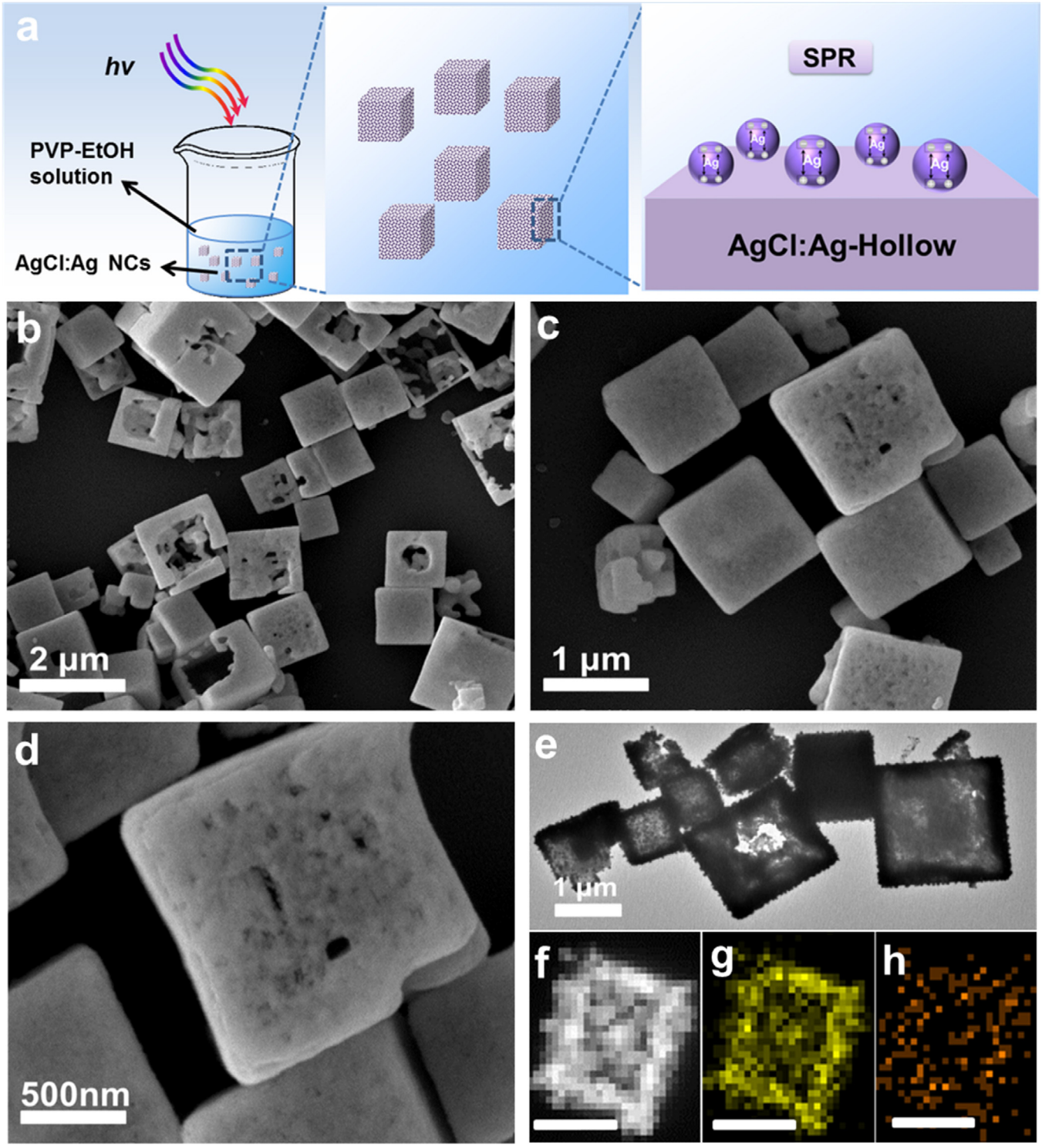

Fig. 1. Electronic images and element distribution images of the AgCl:Ag-Hollow NCs. (a) Schematic illustration of formation of the AgCl:Ag-Hollow NCs. (b–d) The SEM images of the as-prepared AgCl:Ag-Hollow NCs with different resolutions (e) The TEM image of the AgCl:Ag-Hollow NCs. (f–h) High-angle annular dark-field scanning transmission electron microscopy (HAADF-STEM) (f) and element mapping images for Ag (g) and Cl (h) distribution in the AgCl:Ag-Hollow NCs. The scale bar is 200 nm.

species can be attributed to the water dissolution process and the bombardment of high energy electron beam during the SEM and TEM analysis, respectively (Fig. S2 in Supporting information).

The crystallographic structure of as-prepared AgCl:Ag-Hollow NCs and AgCl-Normal materials were determined by means of X-ray diffraction (XRD) analysis (Fig. 2a). XRD pattern of the two samples displayed distinct diffraction peaks at approximately (2θ) 27.7°, 32.2°, 46.2°, 54.8°, 57.5°, 67.5°, 74.4° and 76.7°, which can be assigned to (111), (200), (220), (311), (222), (400), (331) and (420) crystal phases respectively, corresponding to the diffractions of crystalline AgCl (JCPDS file: 31-1238) [24]. As shown in Fig. S3 (in Supporting information), the NaCl@AgCl displayed diffraction peaks (2θ) at 31.9°, 45.7°, 56.7°, 66.4° and 75.5°. These peaks can be assigned to (200), (220), (222), (400) and (420) crystal phases respectively, which was corresponding to the crystal diffraction of NaCl (JCPDS file: 5-0628) [20]. Comparing the XRD

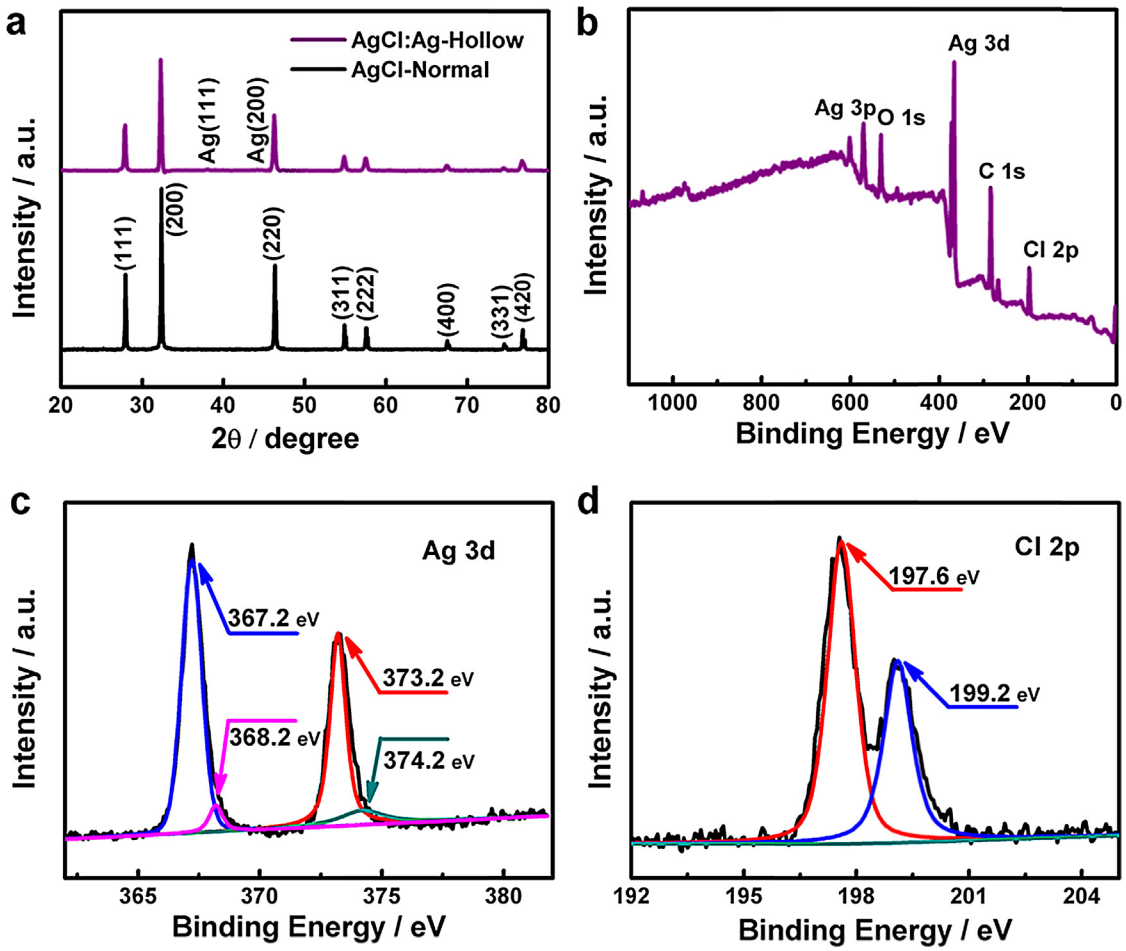

Fig. 2. XRD and XPS characterizations of the AgCl:Ag-Hollow NCs. (a) XRD patterns of the AgCl:Ag-Hollow NCs in comparison with AgCl-Normal materials (JCPDS file: 31-1238). (b–d) The survey XPS spectrum (b), Ag 3d (c) and Cl 2p (d) of the AgCl:Ag-Hollow NCs.

spectra of AgCl and NaCl@AgCl (Fig. S3), it revealed that NaCl core have been completely removed after the water dissolution process. Additionally, as shown in Fig. 2a, the weak diffraction peaks (2θ) at 38.1° and 44.3° were founded in the AgCl:Ag-Hollow NCs, which can be assigned to (1 1 1) and (2 0 0) crystal phases of metallic Ag (JCPDS file: 65-2871). It is noticeable that the Ag^0 NPs were not detected on the surface of AgCl-Normal material due to the very small amount of Ag generated under visible light irradiation process. More specifically, we did not find other characteristic peaks in these two crystal structures, such as impurities or other silver crystal phases, which demonstrated that the obtained product was only composed of metallic Ag and AgCl.

X-ray photoelectron spectroscopy (XPS) was performed to further investigate the surface chemical composition and chemical states of the as-prepared samples (Fig. 2b–d). The survey XPS spectrum (Fig. 2b) of the as-prepared AgCl:Ag-Hollow NCs confirmed the main ingredient elements of Ag and Cl, which agreed well with the results of elemental mapping analysis (Fig. 1e–g). The C 1s and O 1s peaks are probably due to the adventitious hydrocarbon from the XPS instrument itself. Fig. 2c shows that the spectrum of Ag 3d consists of two peaks at 367.2 eV and 373.2 eV, which are ascribed to Ag $3d_{5/2}$ and Ag $3d_{3/2}$, respectively [25]. Furthermore, the peaks of Ag $3d_{5/2}$ and Ag $3d_{3/2}$ could be further divided into different peaks at 367.2 eV, 368.2 eV and 373.2 eV, 374.2 eV, respectively. Namely, the peaks at 367.2 eV and 374.2 eV could be attributed to the peaks of Ag $3d_{5/2}$ of AgCl and Ag $3d_{3/2}$ of metallic Ag^0, whereas the peaks at 368.2 and 373.2 eV could be ascribed to the peaks of Ag $3d_{5/2}$ of metallic Ag^0 and Ag $3d_{3/2}$ of AgCl. For Cl 2p (Fig. 2d), two peaks were obtained at binding energies of 197.6 eV and 199.2 eV, corresponding to Cl $2p_{3/2}$ and Cl $2p_{1/2}$, respectively. All the XPS binding energies coincide well with the reported literature [25,26].

The physical properties and light-absorption properties of the AgCl:Ag-Hollow NCs, AgCl-Normal and commercial P25 were shown in Fig. 3. As shown in Fig. 3a, it can be clearly seen that the dispersion and desiccation of AgCl:Ag-Hollow NCs performed the megascopic purple color, which is conspicuously different from the commonly observed white AgCl-Normal materials (Fig. S4 in Supporting information). Hence, it is supposed that this distinctive coloured NCs would have a doughty absorption in the visible scope.

To authenticate the aforementioned light absorption properties of AgCl:Ag-Hollow NCs, the absorption spectra of these photocatalyst samples were recorded by a UV-Vis spectrophotometer. A strong and broad absorption peak at about 550 nm upon the AgCl:Ag-Hollow NCs was obtained, and its absorption in visible region is much stronger than those of AgCl-Normal and commercial P25 (Fig. 3b). The large absorption improvement of the AgCl:Ag-Hollow NCs can be ascribed to three factors: (i) Except direct absorption on the surface, the incident light could partially get into the inner of the AgCl:Ag-Hollow NCs structure through the outer shell following with several times reflections inside the interior structure, thus greatly enhanced the optical absorption. Namely, this is also the typical property of the porous materials [27]; (ii) In addition, according to concerned literatures, Mie scattering effect of the AgCl:Ag:Hollow NCs also leads to an enhancement of the optical absorption through the increase of average photon path length in the AgCl:Ag:Hollow NCs [28–30]; (iii) Most

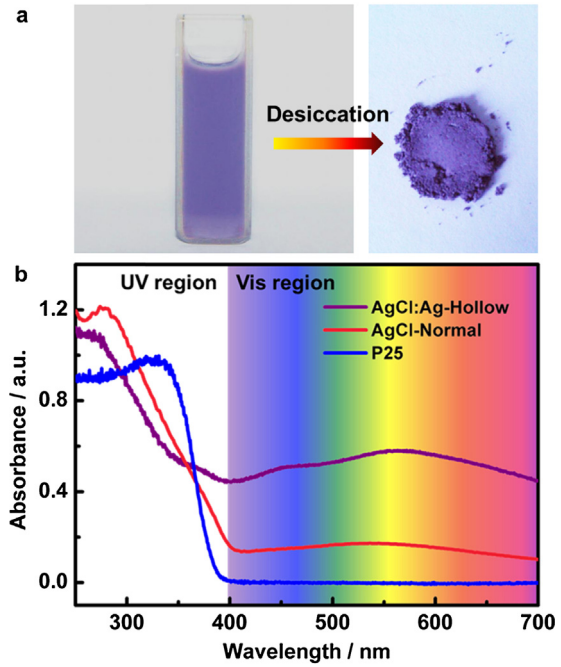

Fig. 3. The physical properties and light absorption properties of the AgCl:Ag-Hollow NCs and AgCl-Normal materials. (a) The digital photographs of dispersion and desiccation of AgCl:Ag-Hollow NCs. (b) UV–visible diffuse reflectance spectra (DRS) of the AgCl:Ag-Hollow NCs, AgCl-Normal and commercial P25.

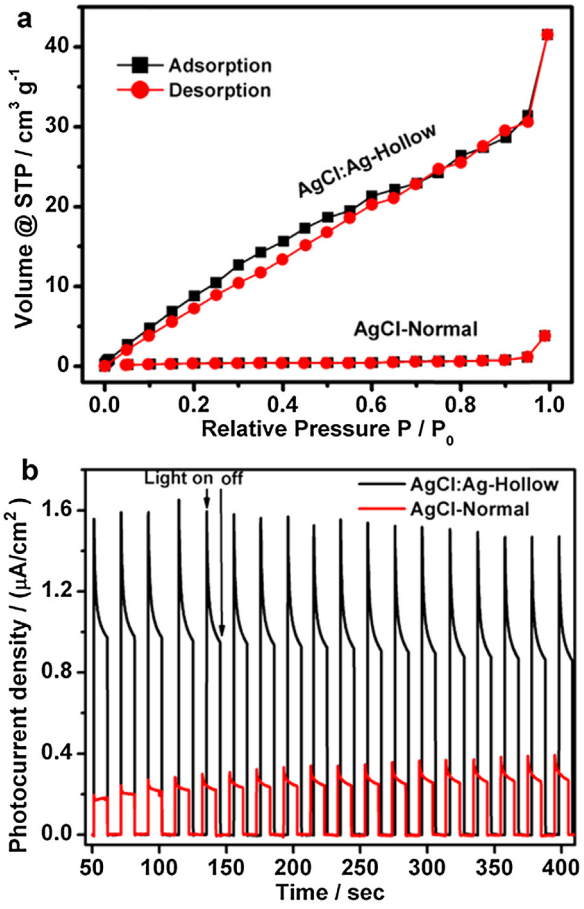

Fig. 4. The BET surface area and photoelectric conversion properties of AgCl:Ag-Hollow NCs and AgCl-Normal. (a) Nitrogen adsorption–desorption isotherms. (b) Photoelectric conversion performances of AgCl:Ag-Hollow NCs and AgCl-Normal materials in 0.1 M Na_2SO_4 aqueous solutions under visible light irradiation ($\lambda > 420$ nm).

importantly, the enhancement could be furthermore ascribed to the localized surface plasmon characteristics of Ag^0 NPs on the surface of AgCl, which were generated under visible light illumination [29,31]. The content of Ag^0 species on the surface of AgCl:Ag-Hollow NCs and AgCl-Normal materials are shown in Fig. S5 (in Supporting information). Commonly, AgCl material has a large band gap (direct band gap: 5.2 eV, indirect band gap: 3.2 eV), which made it show negligible absorption in the visible region [32]. However, such AgCl:Ag-Hollow NCs demonstrated a much smaller band gap value (~2.0 eV, by the band-gap estimation according to Kubelka–Munk theory, shown in Fig. S6 in Supporting information) than AgCl-Normal and commercial P25 materials, which implies a significantly increased light absorption in the visible region [3]. It can further explain the enhanced optical absorption capacity of this AgCl:Ag-Hollow NCs material.

3.2. BET surface area and photoelectrochemical measurements

The Brunauer–Emmet–Teller (BET) surface area and Barrett–Joiner–Halenda (BJH) pore structure of the AgCl:Ag-Hollow NCs and AgCl-Normal materials were investigated by nitrogen adsorption–desorption isotherms (Figs. 4a and S7). The isotherms of the two samples are identified as type IV from the Brunauer–Deming–Deming–Teller (BDDT) classification [33], implying the presence of mesopores (2–50 nm) (Fig. 4a). Furthermore, the desorption branch of the isotherm for AgCl:Ag-Hollow NCs shows a inclined ladder state, which indicted the existence of heterogeneous pore structure. Compared with AgCl-Normal materials, the AgCl:Ag-Hollow NCs show higher adsorption at relative pressures (P/P0) around 1.0. As shown in Fig. S7 (in Supporting information), the formation of large mesopores can be clearly observed and the relative pores size distribution ranged from 2 to over 10 nm. The BET surfaces area of the AgCl:Ag-Hollow NCs and AgCl-Normal materials were calculated to be 58.737 $m^2 g^{-1}$ and 1.382 $m^2 g^{-1}$, respectively. It is obviously found that AgCl:Ag-Hollow NCs presented much higher specific surface area than that of AgCl-Normal, which indicated more photoreduction active sites existing in such AgCl:Ag-Hollow NCs material and they will essentially benefit to photocatalytic reactions.

An excellent material always accompany with many distinctive properties. Of course, the AgCl:Ag-Hollow NCs are of no exception. Herein, photoelectric conversion experiments of the AgCl:Ag-Hollow NCs and AgCl-Normal materials were carried out over several on–off irradiation cycles in Na_2SO_4 aqueous solutions under visible light irradiation (Experimental details were shown in Supporting information). Fig. 4b shows a comparison of the *I–t* curves for these two samples over several on–off cycles of intermittent irradiation. Or rather, the AgCl:Ag-Hollow NCs exhibit a 4–8 times higher photoelectric current and conversion efficiency than that of AgCl-Normal material. The photocurrent value of the AgCl:Ag-Hollow NCs gradually decreased to zero when the irradiation turned off, and would return to a constant value when the light turned on again. By comparison, the photocurrent of AgCl-Normal material rapidly increased or decreased with the light on or off, respectively. Owing to its excellent photo-electric reproducibility, the AgCl:Ag-Hollow NCs showed great potentials in the areas of photodetector, solar cell, fiber-optic communication etc[25]. The photoelectric conversion difference between AgCl:Ag-Hollow NCs and AgCl-Normal material is also consistent with their photocatalytic reduction results in the following discussion.

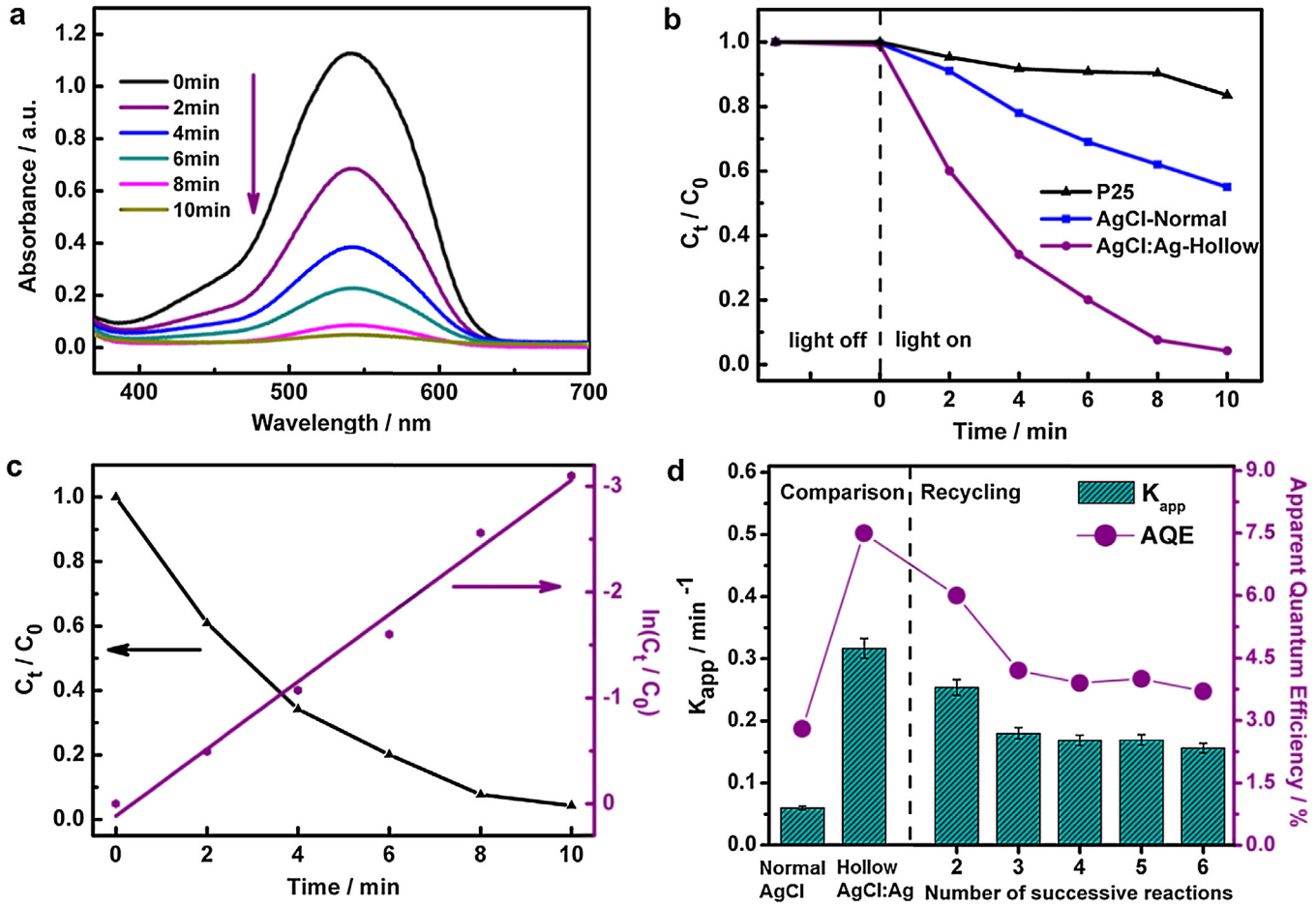

Fig. 5. (a) Time-dependent UV–vis absorption spectra for photoreduction of Cr (VI) ion over AgCl:Ag-Hollow NCs based on the DPC method. (b) Photoreduction dynamic curves for reduction of Cr (VI) ion over commercial P25, AgCl-Normal and AgCl:Ag-hollow NCs. (c) C_t/C_0 and ln(C_t/C_0) against reaction time for photoreduction of Cr (VI) over AgCl:Ag-Hollow NCs. Normally, C_t stands for the concentration of Cr (VI) at time t, C_0 represents to the initial Cr (VI) concentration (10 mg L^{-1}). (d) k_{app} and AQE of different photocatalyst and the number of successive reaction employing AgCl:Ag-Hollow NCs.

3.3. Evaluation of photocatalytic reduction activity

It is worth mentioning that carcinogenic Cr (VI) ion is a common by-product in the industry processes of electroplating, tanning, and fine chemical manufacturing. The most important thing is that heavy metal Cr (VI) ions have long-term adverse impacts to human health and ecosystems due to bioaccumulation as well as biomagnication. The effective conversion of toxic Cr (VI) into the benign form would benefit both environment protection and human healthy. To our knowledge, the carcinogen of Cr (VI) could be reduced to Cr (III) by photocatalysis, and the mechanism of which has been previously reported [11,21]. Briefly, the Cr (VI) and diphenylcarbazide (DPC) in acid solution would generate a violet complex compound, which displays a characteristic absorption peak at λ_{max} = 540 nm. Herein, the variation in the content of Cr (VI) will be equivalent to the concentration changing of the violet complex compound [9].

Fig. 5a presents the UV–vis absorption spectra of the complex compound during the photoreduction process of Cr (VI) over the AgCl:Ag-Hollow NCs. It is clearly seen that the concentration of Cr (VI) decreased with the increased irradiation time and had a sudden-drop from start to 2 min irradiation, while nearly half amount of Cr (VI) was reduced within 4 min irradiation. After 10 min, Cr (VI) ion in the reaction solution could not be detected. Fig. S8 (in Supporting information) shows the typical photograph of color decay from violet to pale (before and during the conversion of Cr (VI) form 0 to 10 min), which indicated the successful photoreduction of Cr (VI). Fig. 5b displays photoreduction dynamic curves over commercial P25, AgCl-Normal and AgCl:Ag-hollow NCs. Under visible irradiation, the AgCl:Ag-hollow NCs exhibit higher Cr (VI) reduction activity than both AgCl-Normal and commercial P25 materials. It is more convincing that Cr (VI) was fully reduced after 10 min irradiation by employing AgCl:Ag-hollow NCs as photocatalyst, while only 44.7% and 16.5% of Cr(VI) was reduced over AgCl-Normal and commercial P25, respectively. The control experiments revealed that the concentration of Cr (VI) remain unchanged in the presence of AgCl:Ag-hollow NCs without irradiation or under irradiation but without catalysts (data not shown).

Photocatalytic reduction kinetics was monitored by the variation of Cr (VI) concentration (Fig. 5c). Furthermore, ln(C_t/C_0) (corresponding to ln(A_t/A_0), where A represents to the absorbance) against the reaction time for photoreduction exhibits a linear relationship and the kinetic study is described by pseudo-first order equation [8,19], which can be expressed as following:

$$\ln\left(\frac{C_0}{C_t}\right) = k_{app}t$$

where C_t is the concentration of Cr (VI) at irradiation time t, C_0 is the initial concentration of Cr (VI). Then, k_{app} is the apparent reaction rate constant, which can be obtained from the slope of the liner correlation [34]. As shown in Fig. 5d, the k_{app} of AgCl:Ag-Hollow NCs and AgCl-Normal were calculated to be 0.317 min^{-1} and 0.06 min^{-1}, respectively. Significantly, the stability and recyclability of AgCl:Ag-Hollow NCs would also play the key role for practical applications. The plots of k_{app} against the number of successive

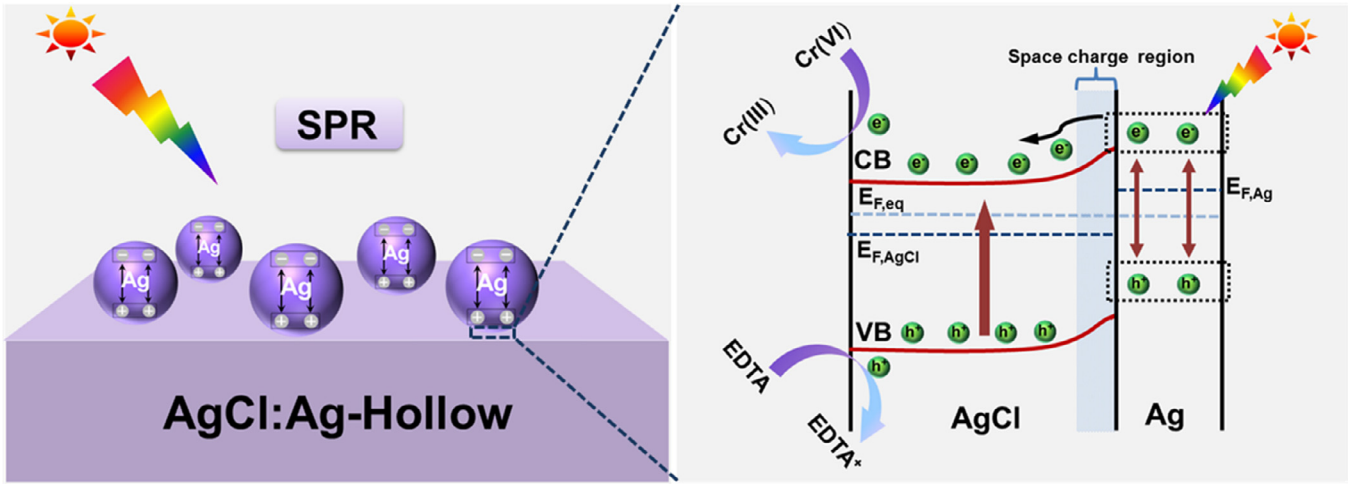

Fig. 6. Schematic diagram illustrating the production of Ag NPs on AgCl and the proposed plasmon-enhanced photoreduction mechanism of Cr (VI) over AgCl:Ag-Hollow NCs.

reduction reactions for repeated using of AgCl:Ag-Hollow NCs were shown in Fig. 5d. It is noticed that the catalytic efficiency only has a little shrinkage which can be attributed to a small mass loss during the reclaim of photocatalyst in recycling reaction process. SEM, TEM and XRD analysis of this AgCl:Ag-Hollow NCs material after several photoreductions were also performed and the results were depicted in Fig. S9 and S10 (in Supporting information). It illustrated that both the morphology and the crystal structure of such AgCl:Ag-Hollow NCs material did not significantly changed. Moreover, the apparent quantum efficiency (AQE) of Cr (VI) photoreduction reaction within 6 min was also calculated. The number of photons was estimated by means of the ferrioxalate actinometer method [11,35] (the experiment details can be found in Supporting information). The results showed that the AQE of the AgCl:Ag-Hollow NCs reached 7.5%, which presented much higher than that of the AgCl-Normal materials (2.8%).

3.4. Hypothesis of photocatalytic reduction mechanism

According to the above experimental results, it is confirmed that the carcinogenic Cr (VI) ions can be essentially photoreduced over the AgCl:Ag-Hollow NCs within 10 min. Furthermore, it is also crucial and necessary to discuss the possible reaction mechanisms which are proposed to explain the enhanced photocatalytic activity as well as the detailed reduction process. Commonly, the AgCl crystal can generate an electron–hole pair and the electron will combine with an Ag^+ to form an Ag^0 species after absorbing a photon under visible light irradiation [29]. Then, Ag^0 nanoclusters will form on the surface of AgCl hollow NCs upon repeated absorption of photons. Simultaneously, under irradiation, the electrons would be generated in the Ag NPs and forced far away from the AgCl interfaces because of the SPR effect of the Ag NPs and polarization field of the AgCl, respectively [32] (Fig. 6, left). What's more, the migration of photo-excited electrons away from the AgCl also prevents photolysis of AgCl to Ag^0 nanoclusters, which finally insured the high stability of the AgCl:Ag-Hollow NCs [36].

Subsequently, as shown in Fig. 6(right), the free electrons of the Ag^0 nanoclusters would prefer to flow to the n-type AgCl semiconductor due to their different work function [37] (Φ_{Ag} = 4.26 eV[36], Φ_{AgCl} = 6.3 eV [38]). According to the previous report, the electrons will transfer from the material with low work function to whom with high work function and accumulate in the space charge region until the two systems run up to equilibrium and form the equilibrated Fermi level [39,40] ($E_{F,Ag}$, $E_{F,AgCl}$ and $E_{F,eq}$). Under this equilibrium, a Schottky barrier would be formed at the junction interface between semiconductor AgCl and Ag NPs [37,41]. The numerous nanoscale quasi-Helmholtz double layers would establish near the interface and tend to interfere coherently to achieve a long range enhanced local electromagnetic field, and then give rise to a upward bending in the band edges [39,42,43]. Stand to reason, the Schottky junction could facilitate the photo-induced carriers separation, which can benefit to suppress recombination of the electron–hole [31,44].

When photoreduction of Cr (VI) reaction is carried out under visible light irradiation, a number of increased electrons will store in the Ag NPs and thus lifted the Fermi energy level of Ag, which were produced by photo-excitation [36]. And the incremental electron density will disequilibrates the Fermi level of the system [45]. Afterwards, the superfluous electrons would be injected into the conduction band (CB) of the neighbouring AgCl until the Fermi level of the systems runs up to equilibrium again (Fig. 6, right). This repeated process not only stabilizes the system equilibrium, but also efficiently facilitate the separation of electron–hole [15,39]. Meanwhile, the enriched photo-excited electrons on the surface of AgCl could be trapped by Cr (VI) ions in solution to form Cr (III), whereas the holes on the valence band (VB) of AgCl would be scavenged by EDTA (a hole scavenger) to form $EDTA^+$ [21]. In addition, the higher photoreduction activity that performed over the AgCl:Ag-Hollow NCs photocatalyst can also be ascribed to its larger surface area, which provides copious active sites for catalysis. All in all, the light absorption, coefficient of utilization, hollow structure, the Schottky junction, SPR-effect, generation and separation of photo-induced charge carriers, interaction with molecules together contribute to the photoactivity enhancement of AgCl:Ag-Hollow system.

4. Conclusions

In summary, the carcinogenic Cr (VI) has been highly efficient photoreducted very fast over eco-friendly as well as robust AgCl:Ag hollow NCs in aqueous solution. And thus it is of paramount significance for both the human health and environmental conservation. Simultaneously, such AgCl:Ag-Hollow photocatalytic reduction agent plays a crucial role in this process. The formation of remarkable heterostructure between Ag and AgCl effectively facilitates charge carrier transfer, which resulted in extremely high activity and stability in photoreduction of carcinogenic Cr (VI). The high performance of catalytic activity should arise from the

following factors: (i) the SPR-effects not only drastically enhanced the visible-light harvesting, but also created an intensive local electric field which significantly facilitates the photocatalytic reactions; (ii) the Schottky junction between Ag NPs and AgCl could facilitate the charge separation, which further benefit to suppress the recombination of electron–holes; (iii) The hollow structure could significantly enhance the light absorption by multiple reflections in the interior structure, and amplified specific surface area (42 times than normal AgCl material). As expected, the apparent kinetic rate constant (k_{app}) and apparent quantum efficiency (AQE) of the AgCl:Ag-Hollow NCs are of 0.317 min^{-1} and 7.5% (within 6 min), respectively. And it demonstrated 5.3 and 2.7 times higher than the normal Ag/AgCl material. It is expected that this class of AgCl-based photocatalyst provides a novel perspective for understanding the mechanism of photocatalytic reduction Cr (VI). Thanks greatly to its environmental friendly solvent and handy preparation approach for AgCl:Ag-Hollow NCs, this kind of photocatalyst might have a wide perspective in mass production and become a promising candidate for practical application of water cleansing and environmental pollution purifying under visible light irradiation in the future.

Acknowledgements

The authors are most grateful to the NSFC, China (No. 21205112, No. 21225524, No. 21475122 and No. 21127006), the Department of Science and Techniques of Jilin Province (No. 20120308, No. 201105031, No. 201215091 and SYHZ0006) and Chinese Academy of Sciences (YZ201354, YZ201355) for their financial support.

Appendix A. Supplementary data

Supplementary data associated with this article can be found, in the online version, at http://dx.doi.org/10.1016/j.apcatb.2014.09.049.

References

[1] D.M. Schultz, T.P. Yoon, Science 343 (2014) 1239176.
[2] X. Chen, S. Shen, L. Guo, S.S. Mao, Chemical Reviews 110 (2010) 6503–6570.
[3] Q. Xiang, B. Cheng, J. Yu, Applied Catalysis B: Environmental 138–139 (2013) 299–303.
[4] Y. Chen, J. Zhang, M. Zhang, X. Wang, Chemical Science 4 (2013) 3244.
[5] J.M. Meichtry, C. Colbeau-Justin, G. Custo, M.I. Litter, Applied Catalysis B: Environmental 144 (2014) 189–195.
[6] S. Wang, D. Li, C. Sun, S. Yang, Y. Guan, H. He, Applied Catalysis B: Environmental 144 (2014) 885–892.
[7] S. Huang, L. Gu, N. Zhu, K. Feng, H. Yuan, Z. Lou, Y. Li, A. Shan, Green Chemistry 16 (2014) 2696.
[8] Y. Yang, G. Wang, Q. Deng, D.H.L. Ng, H. Zhao, ACS Applied Materials & Interfaces 6 (2014) 3008–3015.
[9] J. Shang, W. Hao, X. Lv, T. Wang, X. Wang, Y. Du, S. Dou, T. Xie, D. Wang, J. Wang, ACS Catalysis (2014) 954–961.
[10] Q. Wang, X. Chen, K. Yu, Y. Zhang, Y. Cong, Journal of Hazardous Materials 246-247 (2013) 135–144.
[11] B. Cai, J. Wang, S. Gan, D. Han, Z. Wu, L. Niu, Journal of Materials Chemistry A 2 (2014) 5280.
[12] L. Wang, N. Wang, L. Zhu, H. Yu, H. Tang, Journal of Hazardous Materials 152 (2008) 93–99.
[13] P. Mohapatra, S.K. Samantaray, K. Parida, Journal of Photochemistry and Photobiology A: Chemistry 170 (2005) 189–194.
[14] B. Cai, J. Wang, D. Han, S. Gan, Q. Zhang, Z. Wu, L. Niu, Nanoscale 5 (2013) 10989–10995.
[15] H. Kisch, Angewandte Chemie 52 (2013) 812–847.
[16] H. Tong, S. Ouyang, Y. Bi, N. Umezawa, M. Oshikiri, J. Ye, Advanced Materials 24 (2012) 229–251.
[17] C. Yu, G. Li, S. Kumar, K. Yang, R. Jin, Advanced Materials 26 (6) (2013) 892–898.
[18] R. Marschall, Advanced Functional Materials 24 (2014) 2421–2440.
[19] C. An, S. Peng, Y. Sun, Advanced Materials 22 (2010) 2570–2574.
[20] Y. Tang, Z. Jiang, G. Xing, A. Li, P.D. Kanhere, Y. Zhang, T.C. Sum, S. Li, X. Chen, Z. Dong, Z. Chen, Advanced Functional Materials 23 (2013) 2932–2940.
[21] P. Wang, B. Huang, X. Zhang, X. Qin, Y. Dai, Z. Wang, Z. Lou, ChemCatChem 3 (2011) 360–364.
[22] D. Chen, S.H. Yoo, Q. Huang, G. Ali, S.O. Cho, Chemistry 18 (2012) 5192–5200.
[23] M.R. Jones, K.D. Osberg, R.J. Macfarlane, M.R. Langille, C.A. Mirkin, Chemical Reviews 111 (2011) 3736–3827.
[24] B. Ma, J. Guo, W.-L. Dai, K. Fan, Applied Catalysis B: Environmental 130–131 (2013) 257–263.
[25] L. Han, Z. Xu, P. Wang, S. Dong, Chemical Communications 49 (2013) 4953–4955.
[26] J. Jiang, L. Zhang, Chemistry 17 (2011) 3710–3717.
[27] Y. Li, Y. Ding, The Journal of Physical Chemistry C 114 (2010) 3175–3179.
[28] S. Linic, P. Christopher, D.B. Ingram, Nature Materials 10 (2011) 911–921.
[29] X. Zhang, Y.L. Chen, R.S. Liu, D.P. Tsai, Reports on progress in physics, Physical Society 76 (2013) 046401.
[30] X. Xu, C. Randorn, P. Efstathiou, J.T. Irvine, Nature Materials 11 (2012) 595–598.
[31] W. Hou, S.B. Cronin, Advanced Functional Materials 23 (2013) 1612–1619.
[32] R. Dong, B. Tian, C. Zeng, T. Li, T. Wang, J. Zhang, The Journal of Physical Chemistry C 117 (2013) 213–220.
[33] J. Wang, A.-H. Lu, M. Li, W. Zhang, Y.-S. Chen, D.-X. Tian, W.-C. Li, ACS Nano 7 (2013) 4902–4910.
[34] H. Li, S. Gan, D. Han, W. Ma, B. Cai, W. Zhang, Q. Zhang, L. Niu, Journal of Materials Chemistry A 2 (2014) 3461.
[35] M. Schiavello, V. Augugliaro, V. Loddo, M. Lopez-Munoz, L. Palmisano, Research on Chemical Intermediates 25 (1999) 213–227.
[36] J. Jiang, H. Li, L. Zhang, Chemistry 18 (2012) 6360–6369.
[37] R. Jiang, B. Li, C. Fang, J. Wang, Advanced Materials (2014), http://dx.doi.org/10.1002/adma.201400203.
[38] A. Goldmann, in: A. Goldmann (Ed.), Noble Metals, Noble Metal Halides and Nonmagnetic Transition Metals, Springer, Berlin/Heidelberg, 2003, pp. 125–132.
[39] Z. Zhang, J.T. Yates Jr., Chemical Reviews 112 (2012) 5520–5551.
[40] Y. Tian, T. Tatsuma, Journal of the American Chemical Society 127 (2005) 7632–7637.
[41] C. Clavero, Nature Photonics 8 (2014) 95–103.
[42] A.W. Bott, Current Separations 17 (1998) 87–92.
[43] G.C. Schatz, Accounts of Chemical Research 17 (1984) 370–376.
[44] R. Long, K. Mao, M. Gong, S. Zhou, J. Hu, M. Zhi, Y. You, S. Bai, J. Jiang, Q. Zhang, X. Wu, Y. Xiong, Angewandte Chemie 126 (12) (2014) 3269–3273.
[45] J.W. Ha, T.P. Ruberu, R. Han, B. Dong, J. Vela, N. Fang, Journal of the American Chemical Society 136 (2014) 1398–1408.